THE JOURNAL OF PHYSICAL CHEMISTRY Letters

Letter

Cite This: J. Phys. Chem. Lett. 2018, 9, 4053−4058

pubs.acs.org/JPCL

Vibrationally Assisted Intersystem Crossing in Benchmark Thermally Activated Delayed Fluorescence Molecules

Emrys W. Evans,[†,⊥] Yoann Olivier,[‡,⊥] Yuttapoom Puttisong,[†,⊥] William K. Myers,[§] Timothy J. H. Hele,[†] S. Matthew Menke,[†] Tudor H. Thomas,[†] Dan Credgington,[†] David Beljonne,[‡] Richard H. Friend,[†] and Neil C. Greenham*[,†]

[†]Cavendish Laboratory, University of Cambridge, J. J. Thomson Avenue, Cambridge CB3 0HE, United Kingdom

[‡]Laboratory for Chemistry of Novel Materials, University of Mons, Place du Parc 20, B-7000 Mons, Belgium

[§]Centre for Advanced Electron Spin Resonance (CAESR), University of Oxford, South Parks Road, Oxford OX1 3QR, United Kingdom

Supporting Information

ABSTRACT: Electrically injected charge carriers in organic light-emitting devices (OLEDs) undergo recombination events to form singlet and triplet states in a 1:3 ratio, representing a fundamental hurdle for achieving high quantum efficiency. Dopants based on thermally activated delayed fluorescence (TADF) have emerged as promising candidates for addressing the spin statistics issue in OLEDs. In these materials, reverse singlet−triplet intersystem crossing (rISC) becomes efficient, thereby activating luminescence pathways for weakly emissive triplet states. However, despite a growing consensus that torsional vibrations facilitate spin−orbit-coupling- (SOC-) driven ISC in these molecules, there is a shortage of experimental evidence. We use transient electron spin resonance and theory to show unambiguously that SOC interactions drive spin conversion and that ISC is a dynamic process gated by conformational fluctuations for benchmark carbazolyl−dicyanobenzene TADF emitters.

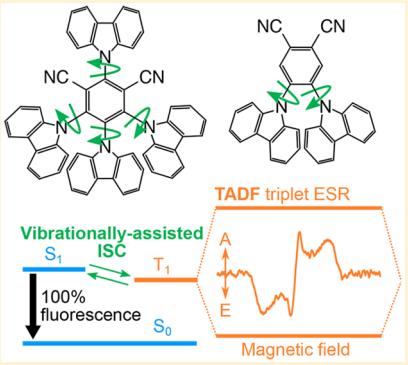

The important role of spin in optoelectronics for organic systems has long been recognized, and in a nutshell, triplet states (T_1) are best avoided. Triplet states provide unwanted loss pathways for charge generation in photovoltaics,[1] and their generally nonemissive nature is at the heart of the classical 25% maximum quantum efficiency limit for OLEDs. Many strategies have been developed to deal with the triplet problem, with much attention since 2012 given to molecules exhibiting thermally activated delayed fluorescence (TADF).[2−8] The name of this phenomenon has been widely adopted in optoelectronics and is equivalent to E-type delayed fluorescence.

Typically, dopants based on TADF have been designed to have a small singlet−triplet energy splitting (ΔE_{ST}). By this scheme, luminescence can be thermally activated from otherwise dark triplet states by efficient intersystem crossing to the emissive singlet excited state (S_1). The simple design rule has led to the discovery of a multitude of molecules exhibiting TADF and a highly active field of research. In general, systems with small ΔE_{ST} are associated with S_1 and T_1 having high charge-transfer (CT) character in which the hole and electron densities are spatially separated, either within the same molecule (e.g., 4CzIPN, 2CzPN, TXO-TPA, and PIC-TRZ)[2,9,10] or between molecules (e.g., m-MTDATA:3T-PYMB).[11] However, despite much success by following this principle, open questions remain as to the mechanism for intersystem crossing and how TADF might be best realized.[12]

Among many notable efforts to understand the general spin interconversion mechanism, Etherington et al. highlighted El-Sayed's rule to explain that pure CT states cannot undergo spin conversion mediated by spin−orbit coupling (SOC) interactions.[13] A "spin-vibronic" mechanism is suggested whereby the T_1 state can be vibronically coupled to other triplet states of high local excited (LE) character. It is important that the higher-lying states have electronic wave functions which lead to significant (and thereby, nonzero) SOC matrix elements with S_1. Overall, mixing of the higher-lying triplet states into the T_1 wave function enables efficient interconversion with S_1.[14,15]

The spin-vibronic model is supported by computational studies combining molecular dynamics (MD) simulations and time-dependent density functional theory calculations within the Tamm−Dancoff approximation (TDA-DFT) which enables a fully atomistic representation of TADF emitters in the solid state as well as a characterization of their lowest singlet and triplet excited states.[16] It was found that the S_1 and T_1 adiabatic states have a strongly mixed CT/LE character,

Received: May 17, 2018
Accepted: June 29, 2018
Published: June 29, 2018

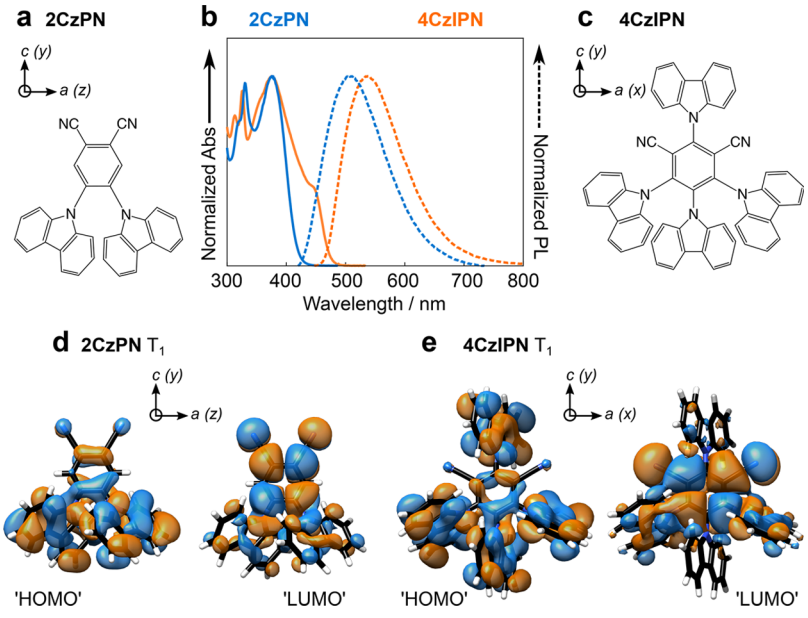

Figure 1. Chemical structures for (a) 2CzPN and (c) 4CzIPN. (b) UV−vis absorption (abs) and photoluminescence (PL) spectra for 100 μM 2CzPN (blue)/4CzIPN (orange) in toluene. UKS-DFT-calculated canonical orbitals for the T_1 states of (d) 2CzPN and (e) 4CzIPN, using the PBE0 functional and EPR-II basis set. *a*, *b*, and *c* and *x*, *y*, and *z* denote the symmetry and ZFS axes, respectively.

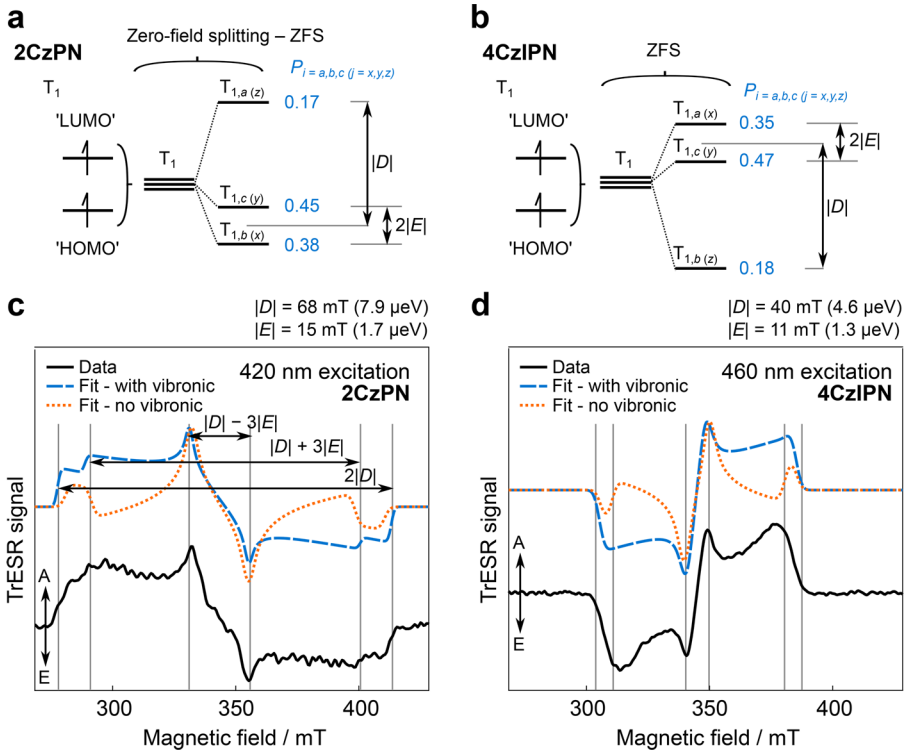

Figure 2. Zero-field splitting (ZFS) diagram for (a) prolate 2CzPN and (b) oblate 4CzIPN, indicating fitted |*D*| and |*E*| parameters. TrESR spectra (80 K) for toluene solutions of 2CzPN (420 nm excitation) and 4CzIPN (460 nm excitation) with black solid lines in parts c and d. Spectra were recorded 0.4 μs after laser excitation (0.04 μs averaged). Vertical lines overlaid on the spectra denote canonical orientations of the magnetic field with respect to the ZFS principal axes, and can be used to derive |*D*| and |*E*| as shown in part c. Fits "with vibronic" and for "no vibronic" contributions to ISC are given.

with the extent of mixing depending on the instantaneous molecular conformation, i.e. the torsion angle between the electron-donating and -accepting units. The CT/LE character was quantified by computing the overlap index ϕ_S within the attachment/detachment formalism[17] (for pure, "ionic" CT, $\phi_S \rightarrow 0$; for pure LE, $\phi_S \rightarrow 1$). It emerged that the time-dependent CT/LE character of excited states results in time-dependent SOC matrix elements and ΔE_{ST}, leading to gated S_1-T_1 spin conversion.

It is worth emphasizing that coupling to vibrational modes plays a significant role in SOC-mediated ISC for a number of systems with large exchange energies, ranging from anthra-

DOI: 10.1021/acs.jpclett.8b01556
J. Phys. Chem. Lett. 2018, 9, 4053−4058

cene[18,19] and porphyrins[20] to chlorophyll[21] and nitrogen-vacancy diamond centers[22] (in the guise of phonons). As the role of vibronic coupling in mediating intersystem crossing for TADF becomes more widely accepted, it is noteworthy that there is a shortage of direct, experimental evidence (see review by Penfold et al.[23]) to counter claims that nuclear-electron hyperfine interactions mediate ISC in such systems with low exchange energies.[24] In one example, Etherington et al. suggested that the TADF luminescence intensity is maximized when S_1 and a ^{3}LE (T_2) triplet are degenerate.[13] Similarly, coupling of the ^{1}CT (S_1) to the ^{3}LE state was considered by Hosokai et al. to be the determining factor as to whether or not different carbazolyl-dicyanobenzene derivatives exhibiting near-identical ΔE_{ST} (= 0.2 eV $\gg kT$) demonstrated appreciable TADF.[25]

Here we use transient electron spin resonance (TrESR) to explore the mechanism of spin mixing of S_1 and T_1 states in molecules exhibiting TADF. Our experimental results provide clear evidence for SOC-mediated intersystem crossing triggered by thermally populated soft (torsional) vibrational modes. Furthermore, the experiments can be rationalized by simple group theory considerations and conformational analysis.[16]

1,2,3,5-Tetrakis(carbazol-9-yl)-4,6-dicyanobenzene (4CzIPN) and 1,2-bis(carbazol-9-yl)-4,5-dicyanobenzene (2CzPN) were selected for this study as they belong to the aforementioned class of carbazolyl−dicyanobenzene derivatives first presented by Uoyama et al. in the seminal TADF paper.[2] These molecules are often considered to be a "benchmark" for TADF OLEDs due to their short radiative lifetimes and high quantum efficiency in devices. 4CzIPN has been found to out-perform 2CzPN; this has been attributed to ΔE_{ST} of 0.04 eV for the former material and 0.21 eV for the latter. Chemical structures for 4CzIPN and 2CzPN are given in Figure 1a,c, together with the coordinate designation used herein (*a*, *b*, and *c* for the symmetry axes where *c* corresponds to the C_2 axis; and *x*, *y*, and *z* for the principal zero-field splitting (ZFS) axes of the triplet state). For reference, normalized UV−vis absorption and photoluminescence spectra for 100 μM solutions in toluene are shown in Figure 1b.

TrESR is an attractive tool for investigating TADF molecules as the relevant triplet states with CT and LE character are paramagnetic, and can be monitored with nanosecond temporal resolution following photoexcitation.[26] The spin substates of these species are energetically split with a magnetic field. The energy separations can be probed as resonances using a CW microwave source at a fixed frequency, ~9.5 GHz. In the TrESR experiment, the magnetic field is varied and a 2D map of temporal and spectral information was recorded by direct detection of microwave absorption and emission with a transient recorder. ESR spectral shapes are dictated by the spin−spin interactions and interspin distances, *r*. Generally, the width of the ESR spectrum follows a $1/r^3$ dependence and will be discussed in more detail later. Ogiwara et al. have previously examined TADF molecules (including 4CzIPN) using TrESR.[24] Intriguingly, the best device performance was found to correlate with TADF molecules which undergo intersystem crossing driven by hyperfine interactions—this being the dominant pathway found for 4CzIPN.

TrESR spectra (0.4 μs after pulsed laser excitation, 80 K) for flash-frozen ~500 μM samples of 4CzIPN and 2CzPN in toluene are given in Figure 2c,d, showing relatively broad, polarized signals. Unpolarized light was used in photoexcitation. The absorption (A)/emission (E) phase pattern of the ESR spectra arises as the triplets form in a non-Boltzmann population of their sublevels following intersystem crossing. An AAAEEE polarization pattern is found for 2CzPN, while a narrower EEEAAA signal is seen for 4CzIPN. Both patterns are characteristic for ISC mediated by SOC interactions,[27] and not the hyperfine mechanism as was previously suggested;[24] the hyperfine mechanism leads to triplet signals with exclusively AEEAAE or EAAEEA polarization patterns.[27]

In contrast to the previous TrESR experiments,[24] selective photoexcitation for the lowest-energy absorption bands associated with 2CzPN (420 nm) and 4CzIPN (460 nm) was used (cf. Figure 1b). We consider that this condition realizes excited states which are most comparable to those formed at dopant centers following charge recombination. However, we also note that replicating the stated experimental conditions used by Ogiwara et al. (10 μM conc. in toluene and sample excitation at 355 nm) also gave rise to an EEEAAA signal for 4CzIPN. Again, our results are in contrast to the previous study (see Figure S1), and thereby warrant reinterpretation of the spin polarization implications for ISC in 4CzIPN.

TrESR density plots for the ESR signals with respect to magnetic field and time can be found in the Supporting Information (Figure S2), showing that the polarized triplet signals decay over several microseconds due to a combination of triplet lifetime and spin relaxation effects.

As mentioned above, the width of the triplet state ESR spectrum depends on interactions between electron spins. In more detail, for all-organic molecules, these are magnetic dipole−dipole interactions which lift the degeneracy of the triplet sublevels even in the absence of magnetic field (see Figure 2a,b). This effect is termed the zero-field splitting (ZFS) and is described by the following Hamiltonian:

$$\hat{H}_{ZFS} = D\left(\hat{S}_z^2 - \frac{1}{3}\hat{\mathbf{S}}^2\right) + E(\hat{S}_x^2 - \hat{S}_y^2)$$

where $\hat{\mathbf{S}}$ is the total spin angular momentum operator ($\hat{\mathbf{S}} = [\hat{S}_x, \hat{S}_y, \hat{S}_z]$, with $\hat{S}_i$ corresponding to the operator for the *i*-component of the spin angular momentum); $D = \frac{3}{2}D_z$ and $E = \frac{1}{2}(D_x - D_y)$, with $|D_y| \leq |D_x| < |D_z|$ being the principal values for the ZFS interaction tensor.

The nodes observed in the TrESR spectra are highlighted in Figure 2c,d, and correspond to canonical orientations of the magnetic field with respect to the principal axes of the ZFS tensor. Consequently, it is possible to infer the magnitude of the ZFS interaction parameters directly from the ESR spectra as indicated in Figure 2c. For 2CzPN, $|D|$ = 68 mT (7.9 μeV), $|E|$ = 15 mT (1.7 μeV); for 4CzIPN $|D|$ = 40 mT (4.6 μeV), $|E|$ = 11 mT (1.3 μeV).

We have investigated the nature of T_1 states (i.e., associated spin distribution, ZFS tensor) with density functional theory (DFT) calculations using the PBE0 exchange-correlation functional and EPR-II basis set.[26,28,29] The geometry-optimized T_1 states for 2CzPN (Figure 1d) and 4CzIPN (Figure 1e) are depicted with associated hole- "HOMO" and electron- "LUMO". It is apparent that the triplet orbitals are spread across the entirety of the molecules, overlapping at the central benzene group (Figure 1d,e). Explicit calculations of

DOI: 10.1021/acs.jpclett.8b01556
J. Phys. Chem. Lett. 2018, 9, 4053−4058

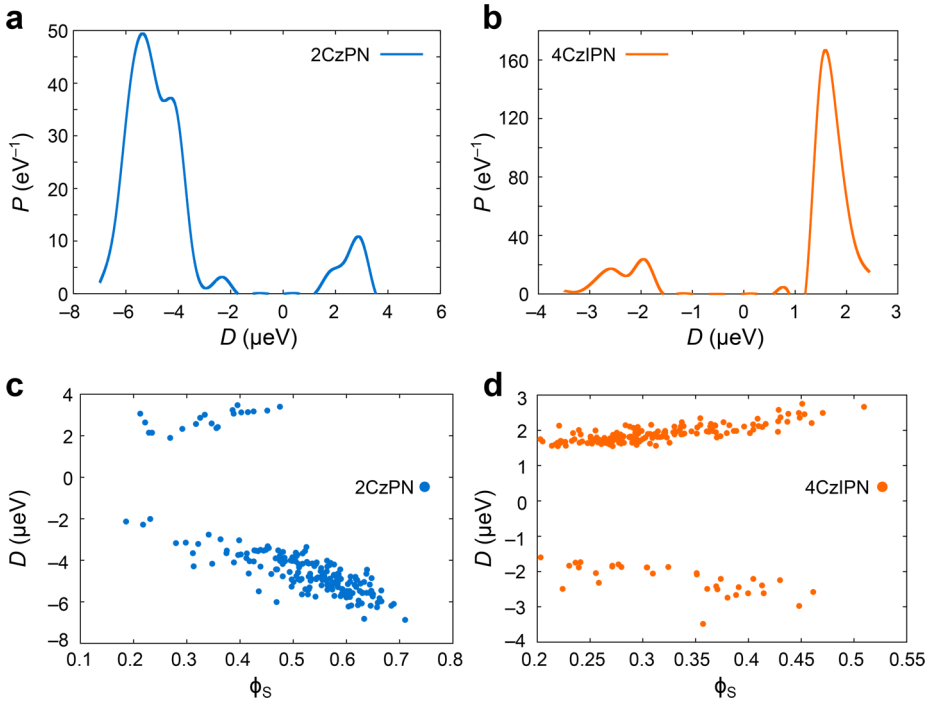

Figure 3. Probability distributions for the zero-field splitting (ZFS) D parameter for (a) 2CzPN and (b) 4CzIPN, obtained from DFT calculations (UKS) using the PBE0 functional and the EPR-II basis set based on a set of 200 molecular geometries extracted from 300 K molecular dynamics simulations. Plots of D versus overlap index (ϕ_S) for (c) 2CzPN and (d) 4CzIPN.

Table 1. Spin−Orbit Coupling Matrix Elements for *a*-, *b*-, and *c*-Components As Defined in the Coordinate System Indicated in Figure 1a,c[a]

	static, 0 K, SOC matrix elements (meV)			dynamic, 300 K, mean and standard deviation of SOC matrix elements (meV)		
	SOC_a	SOC_b	SOC_c	$\mu(SOC_a) \pm \sigma(SOC_a)$	$\mu(SOC_b) \pm \sigma(SOC_b)$	$\mu(SOC_c) \pm \sigma(SOC_c)$
2CzPN	1.2×10^{-3}	1.3×10^{-4}	6.3×10^{-2}	$1.77 \times 10^{-2} \pm 1.63 \times 10^{-2}$	$1.65 \times 10^{-2} \pm 1.52 \times 10^{-2}$	$4.28 \times 10^{-2} \pm 1.22 \times 10^{-2}$
4CzIPN	1.7×10^{-5}	2.9×10^{-4}	1.9×10^{-2}	$7.46 \times 10^{-3} \pm 5.97 \times 10^{-3}$	$7.15 \times 10^{-3} \pm 7.13 \times 10^{-3}$	$1.08 \times 10^{-2} \pm 7.78 \times 10^{-3}$

[a]The "static, 0 K" calculation was conducted for UKS-DFT, T_1-derived geometries. The "dynamic, 300 K" results were obtained by taking the average and standard deviation for the 200 molecular geometries extracted from one snapshot of 300 K molecular dynamics simulations.

the ZFS parameter D confirm that 2CzPN exhibits a more "rod"-like spin density distribution and thus the characteristic prolate splitting ($D < 0$, Figure 2a) of the triplet sublevels, while 4CzIPN displays a more "disc"-like spin density distribution and an oblate ZFS ($D > 0$, see Figure 2b). In 2CzPN, the long axis of the "rod" follows the assigned a-axis; while for 4CzIPN, which has a more discoid shape, the b-axis is perpendicular to the plane of the disc. Although DFT is a reliable method for prolate/oblate assignment in all-organic systems, the absolute calculated values are known to underestimate ZFS parameters routinely:[30] here, 2CzPN, $|D|$ = 6.9 μeV (calculation) < 7.9 μeV (experiment); 4CzIPN, $|D|$ = 2.2 μeV (calculation) < 4.6 μeV (experiment).

By extending the ZFS calculation to a set of 200 molecular geometries extracted from one snapshot of room-temperature (300 K) molecular dynamics (MD) simulations,[16] we found that prolate and oblate ZFS spin distributions are predominantly observed for 2CzPN (~90%) and 4CzIPN (~82%)—see Figure 3a,b, in agreement with the DFT triplet-state-optimized geometries as obtained with the B3LYP functional and the EPR-II basis set (0 K).[31] We observe that the magnitude of D has a positive correlation with increasing the overlap index ϕ_S, i.e. the LE character (Figure 3c,d). This is intuitively understood by the interspin distance dependence of the ZFS parameter. Because ZFS arises from dipole−dipole interaction, the ZFS parameter D is proportional to $(1-3\cos^2\theta)/r^3$, where r is the interspin distance, and θ is the angle between the interspin vector and the maximum dipolar coupling axis. In a classical picture, the interspin distance is expected to decrease (increase) with increasing LE (CT) character as quantified by ϕ_S supporting the mixed CT-LE nature of the excited states in TADF materials. Analogous plots for E are given in Figure S3 of the Supporting Information.

The population of the different T_1 sublevels immediately after excitation follows the magnitude of the ISC rate from S_1 to the T_1 sublevels. In a Fermi's Golden Rule formalism, the difference in ISC rate is mainly driven by the difference in the expectation value of the spin−orbit coupling matrix elements: $SOC_{a,b,c} = \langle T_{1,i=a,b,c}|\hat{H}_{SOC}|S_1\rangle$ from S_1 to $T_{1,i=a,b,c}$ since the Franck−Condon factors associated with $T_{1,i=a,b,c}$ and S_1 are negligibly different. The ZFS interaction is on the order of ~1−10 μeV, and thus energetics are expected to play a minor role in determining relative ISC rates for the sublevels.

Explicit calculation of the spin−orbit coupling matrix elements for the 0 K geometries found that $SOC_{a,b}$ are much smaller (at least 2 orders of magnitude) than SOC_c—see Table 1. This is understood readily from group theory and symmetry (see Supporting Information) when associating 2CzPN and

DOI: 10.1021/acs.jpclett.8b01556
J. Phys. Chem. Lett. 2018, 9, 4053−4058

4CzIPN to the C_2 symmetry point group and considering c as the polarization axis. Therefore, the populations of $T_{1,a}$ and $T_{1,b}$ are negligible while that of the $T_{1,c}$ sublevel is close to 1. However, when accounting for such population partition among the triplet sublevels, poor fits for simulated TrESR spectra as well as incorrect AEAEAE and EAEAEA polarization patterns are obtained for 2CzPN and 4CzIPN, respectively. Thus, a purely electronic model neglecting higher-order effects associated with vibronic interactions fails, even qualitatively, to reproduce the experimental TrESR data ("Fit − no vibronic" in Figure 2c,d). See Supporting Information for full fit details.

Previously, we have shown that consideration of vibronic coupling in the singlet and triplet manifolds of states was essential when computing ISC rates for TADF materials.[16] More specifically, 2CzPN and 4CzIPN consist of "donor" (i.e., carbazole) and "acceptor" (i.e., cyano-) groups associated with a shared moiety (i.e., a benzene core), with an appreciable amount of torsional freedom available. It was demonstrated that conformational freedom leads to modulation of the instantaneous CT/LE mixing (quantified through overlap index), triggering significant SOC between the singlet and triplet states, and thereby allowing ISC. Thus, vibronic coupling was deemed necessary to reach the compromise between reduced ΔE_{ST} and appreciable SOC matrix elements for reverse ISC ($T_1 \rightarrow S_1$).

In order to assess the role of vibronic interactions on steering the relative populations of the triplet sublevels, we repeated the SOC calculations along the same 300 K classical MD trajectory used for obtaining the geometries examined in Figure 3. As indicated in Table 1, proper sampling of all vibrational degrees of freedom, notably of the torsion modes, largely homogenizes the a-, b-, and c-components of the SOC, and as a result the respective sublevel populations (though a slight c-bias persists). In an analogous manner, the large standard deviation values also indicate that the variation of SOC elements are associated with floppy carbazole torsional modes. Similar to Herzberg−Teller intensity borrowing effects in optical absorption, coupling of the electronic and vibrational degrees of freedom at various orders relaxes the symmetry constraints pertaining to purely electronic processes and is here accounted for in a nonperturbative way.

The experimental ESR data are in line with the SOC matrix elements presented in Table 1. Namely, for the prolate 2CzPN (Figure 2a) and oblate 4CzIPN (Figure 2b) triplet species, the analysis of the polarized ESR signals directly points to non-Boltzmann populations following ISC. Best fits to the data indeed yield near-homogeneous populations of the $T_{1,a}$, $T_{1,b}$, and $T_{1,c}$, but with a slight bias for $T_{1,c}$-sublevel. In more detail, the fractional populations (P) for the sublevels are found to be 2CzPN, $P_a = 0.17$, $P_b = 0.38$, and $P_c = 0.45$; 4CzIPN, $P_a = 0.35$, $P_b = 0.18$, and $P_c = 0.47$. The "fit—with vibronic" values ($P_{i=a,b,c}$) are denoted for the ZFS sublevels in Figure 2a,b, and the fits are plotted in Figure 2c,d. While the fitted populations do not correspond exactly to the results of the dynamic calculations, the same general trends are supported.

Our results indicate that spin−orbit coupling (SOC) interactions drive singlet−triplet ISC in the archetypal 4CzIPN and 2CzPN molecules, even in the absence of heavy metals. Furthermore, the polarization of the observed triplet ESR signals support the proposal of vibronically mediated ISC. Explicit calculation of the SOC matrix elements and group theory considerations support the observed C_2-, c-axis bias following ISC in the triplet sublevel populations. Introduction of torsional freedom to the system is necessary to reproduce the non-negligible spin conversion to the a- and b-levels as observed in experiment, thereby providing definitive and direct evidence for the role of vibronic coupling in spin interconversion. Critically, torsional freedom between the "donor" and "acceptor" moieties in the classical TADF motif enables additional ISC pathways between S_1 and T_1.

■ ASSOCIATED CONTENT

Supporting Information

The Supporting Information is available free of charge on the ACS Publications website at DOI: 10.1021/acs.jpclett.8b01556 The data underlying this paper are available at https://doi.org/10.17863/CAM.23135.

Further experimental details for the TrESR experiments; ESR simulation and experiment details, and additional data; E-distribution from molecular dynamics; and symmetry and group theory considerations for evaluating spin−orbit coupling elements (PDF)

■ AUTHOR INFORMATION

Corresponding Author

*E-mail: ncg11@cam.ac.uk (N.C.G.).

ORCID

Emrys W. Evans: 0000-0002-9092-3938
Yuttapoom Puttisong: 0000-0002-9690-6231
Timothy J. H. Hele: 0000-0003-2367-3825
S. Matthew Menke: 0000-0003-4468-0223
Richard H. Friend: 0000-0001-6565-6308
Neil C. Greenham: 0000-0002-2155-2432

Author Contributions

⊥Denotes an equal contribution.

Notes

The authors declare no competing financial interest.

■ ACKNOWLEDGMENTS

E.W.E., N.C.G. and R.H.F. would like to thank the EPSRC for funding (EP/M01083X/1, EP/M005143/1). Y.P. is grateful to The Swedish Research Council VR2015-00436 for a postdoc grant. W.K.M. is supported by the EPSRC grant EP/L011972/1 for CAESR (Centre for Advanced Electron Spin Resonance). T.J.H.H. thanks Jesus College, Cambridge, for a Research Fellowship. DJNC acknowledges the Royal Society for a University Research Fellowship. The work in Mons was supported by the European Union's Horizon 2020 research and innovation program under Grant Agreement No. 646176 (EXTMOS project) and by Belgian National Fund for Scientific Research (FNRS/F.R.S.). Computational resources have been provided by the Consortium des Équipements de Calcul Intensif (CÉCI), funded by F.R.S.-FNRS under Grant No. 2.5020.11 as well as the Tier-1 supercomputer of the Fédération Wallonie-Bruxelles, funded by the Walloon Region under Grant Agreement No. 1117545. D.B. is a FNRS Research Director. Y.O. acknowledges stimulating discussions with Prof. J. C. Sancho-Garcia from the University of Alicante and Prof. L. Muccioli from the University of Bologna.

■ REFERENCES

(1) Rao, A.; Chow, P. C. Y.; Gélinas, S.; Schlenker, C. W.; Li, C.-Z.; Yip, H.-L.; Jen, A. K. Y.; Ginger, D. S.; Friend, R. H. The Role of Spin

DOI: 10.1021/acs.jpclett.8b01556
J. Phys. Chem. Lett. 2018, 9, 4053−4058

in the Kinetic Control of Recombination in Organic Photovoltaics. *Nature* **2013**, *500*, 435−439.
(2) Uoyama, H.; Goushi, K.; Shizu, K.; Nomura, H.; Adachi, C. Highly Efficient Organic Light-Emitting Diodes from Delayed Fluorescence. *Nature* **2012**, *492*, 234−240.
(3) Tanaka, H.; Shizu, K.; Adachi, C.; et al. Efficient Green Thermally Activated Delayed Fluorescence (TADF) from a Phenoxazine−Triphenyltriazine (PXZ−TRZ) Derivative. *Chem. Commun.* **2012**, *48*, 11392−11394.
(4) Zhang, Q.; Li, B.; Huang, S.; Nomura, H.; Tanaka, H.; Adachi, C. Efficient Blue Organic Light-Emitting Diodes Employing Thermally Activated Delayed Fluorescence. Nat. *Nat. Photonics* **2014**, *8*, 326−332.
(5) Hirata, S.; Sakai, Y.; Masui, K.; Tanaka, H.; Lee, S. Y.; Nomura, H.; Nakamura, N.; Yasumatsu, M.; Nakanotani, H.; Zhang, Q.; et al. Highly Efficient Blue Electroluminescence Based on Thermally Activated Delayed Fluorescence. *Nat. Mater.* **2015**, *14*, 330−336.
(6) Lin, T.; Chatterjee, T.; Tsai, W.; Lee, W.; Wu, M.; Jiao, M.; et al. Sky-Blue Organic Light Emitting Diode with 37% External Quantum Efficiency Using Thermally Activated Delayed Fluorescence from Spiroacridine-Triazine Hybrid. *Adv. Mater.* **2016**, *28*, 6976−6983.
(7) Freeman, D. M. E.; Musser, A. J.; Frost, J. M.; Stern, H. L.; Forster, A. K.; Fallon, K. J.; Rapidis, A. G.; Cacialli, F.; McCulloch, I.; Clarke, T. M.; et al. Synthesis and Exciton Dynamics of Donor-Orthogonal Acceptor Conjugated Polymers: Reducing the Singlet-Triplet Energy Gap. *J. Am. Chem. Soc.* **2017**, *139*, 11073−11080.
(8) Kim, D. H.; D'Aléo, A.; Chen, X. K.; Sandanayaka, A. D. S.; Yao, D.; Zhao, L.; Komino, T.; Zaborova, E.; Canard, G.; Tsuchiya, Y.; et al. High-Efficiency Electroluminescence and Amplified Spontaneous Emission from a Thermally Activated Delayed Fluorescent Near-Infrared Emitter. Nat. *Nat. Photonics* **2018**, *12*, 98−104.
(9) Wang, H.; Xie, L.; Peng, Q.; Meng, L.; Wang, Y.; Yi, Y.; Wang, P. Novel Thermally Activated Delayed Fluorescence Materials-Thioxanthone Derivatives and Their Applications for Highly Efficient OLEDs. *Adv. Mater.* **2014**, *26*, 5198−5204.
(10) Endo, A.; Sato, K.; Yoshimura, K.; Kai, T.; Kawada, A.; Miyazaki, H.; Adachi, C. Efficient Up-Conversion of Triplet Excitons into a Singlet State and Its Application for Organic Light Emitting Diodes. *Appl. Phys. Lett.* **2011**, *98*, 083302.
(11) Goushi, K.; Yoshida, K.; Sato, K.; Adachi, C. Organic Light-Emitting Diodes Employing Efficient Reverse Intersystem Crossing for Triplet-to-Singlet State Conversion. Nat. *Nat. Photonics* **2012**, *6*, 253−258.
(12) Wong, M. Y.; Zysman-Colman, E. Purely Organic Thermally Activated Delayed Fluorescence Materials for Organic Light-Emitting Diodes. *Adv. Mater.* **2017**, *29*, 1605444.
(13) Etherington, M. K.; Gibson, J.; Higginbotham, H. F.; Penfold, T. J.; Monkman, A. P. Revealing the Spin−Vibronic Coupling Mechanism of Thermally Activated Delayed Fluorescence. *Nat. Commun.* **2016**, *7*, 13680.
(14) Chen, X.-K.; Zhang, S.-F.; Fan, J.-X.; Ren, A.-M. Nature of Highly Efficient Thermally Activated Delayed Fluorescence in Organic Light-Emitting Diode Emitters: Nonadiabatic Effect between Excited States. *J. Phys. Chem. C* **2015**, *119*, 9728−9733.
(15) Gibson, J.; Monkman, A. P.; Penfold, T. J. The Importance of Vibronic Coupling for Efficient Reverse Intersystem Crossing in Thermally Activated Delayed Fluorescence Molecules. *ChemPhysChem* **2016**, *17*, 2956−2961.
(16) Olivier, Y.; Yurash, B.; Muccioli, L.; D'Avino, G.; Mikhnenko, O.; Adachi, C.; Nguyen, T.-Q.; Beljonne, D.; et al. Nature of the Singlet and Triplet Excitations Mediating Thermally Activated Delayed Fluorescence. *Phys. Rev. Mater.* **2017**, *1*, 75602.
(17) Dreuw, A.; Head-Gordon, M. Single-Reference Ab Initio Methods for the Calculation of Excited States of Large Molecules. *Chem. Rev.* **2005**, *105*, 4009−4037.
(18) Metz, F.; Friedrich, S.; Hohlneicher, G. What Is the Leading Mechanism for the Nonradiative Decay of the Lowest Triplet State of Aromatic Hydrocarbons? *Chem. Phys. Lett.* **1972**, *16*, 353−358.
(19) Metz, F. Position-Dependent Deuterium Effect on Relative Rate Constants for ISC Processes in Aromatic Hydrocarbons. *Chem. Phys. Lett.* **1973**, *22*, 186−190.
(20) van Dorp, W. G.; Schoemaker, W. H.; Soma, M.; van der Waals, J. H. The Lowest Triplet State of Free Base Porphin. *Mol. Phys.* **1975**, *30*, 1701−1721.
(21) Budil, D. E.; Thurnauer, M. C. The Chlorophyll Triplet-State as a Probe of Structure and Function in Photosynthesis. *Biochim. Biophys. Acta, Bioenerg.* **1991**, *1057*, 1−41.
(22) Goldman, M. L.; Sipahigil, A.; Doherty, M. W.; Yao, N. Y.; Bennett, S. D.; Markham, M.; Twitchen, D. J.; Manson, N. B.; Kubanek, A.; Lukin, M. D. Phonon-Induced Population Dynamics and Intersystem Crossing in Nitrogen-Vacancy Centers. *Phys. Rev. Lett.* **2015**, *114*, 1−6.
(23) Penfold, T. J.; Gindensperger, E.; Daniel, C.; Marian, C. M. Spin-Vibronic Mechanism for Intersystem Crossing. *Chem. Rev.* **2018**, DOI: 10.1021/acs.chemrev.7b00617.
(24) Ogiwara, T.; Wakikawa, Y.; Ikoma, T. Mechanism of Intersystem Crossing of Thermally Activated Delayed Fluorescence Molecules. *J. Phys. Chem. A* **2015**, *119*, 3415−3418.
(25) Hosokai, T.; Matsuzaki, H.; Nakanotani, H.; Tokumaru, K.; Tsutsui, T.; Furube, A.; Nasu, K.; Nomura, H.; Yahiro, M.; Adachi, C. Evidence and Mechanism of Efficient Thermally Activated Delayed Fluorescence Promoted by Delocalized Excited States. *Sci. Adv.* **2017**, *3*, e1603282.
(26) Richert, S.; Tait, C. E.; Timmel, C. R. Delocalisation of Photoexcited Triplet States Probed by Transient EPR and Hyperfine Spectroscopy. *J. Magn. Reson.* **2017**, *280*, 103−116.
(27) Hoff, A. J. *Advanced EPR: Applications in Biology and Biochemistry*; Elseveier: Amsterdam, 1989.
(28) Barone, V. *Recent Advances in Density Functional Methods*; World Scientific: Singapore, 1995.
(29) Adamo, C.; Barone, V. Toward Reliable Density Functional Methods without Adjustable Parameters: The PBE0 Model. *J. Chem. Phys.* **1999**, *110*, 6158−6170.
(30) Sinnecker, S.; Neese, F. Spin-Spin Contributions to the Zero-Field Splitting Tensor in Organic Triplets, Carbenes and Biradicals: A Density Functional and Ab Initio Study. *J. Phys. Chem. A* **2006**, *110*, 12267−12275.
(31) Neese, F. The ORCA Program System. *Wiley Interdiscip. Rev. Comput. Mol. Sci.* **2012**, *2*, 73−78.

DOI: 10.1021/acs.jpclett.8b01556
J. Phys. Chem. Lett. 2018, 9, 4053−4058